OXFORD

Human Molecular Genetics, 2015, Vol. 24, No. 25 7196–7206

doi: 10.1093/hmg/ddv417
Advance Access Publication Date: 3 October 2015
Original Article

ORIGINAL ARTICLE

Age-dependent gait abnormalities in mice lacking the *Rnf170* gene linked to human autosomal-dominant sensory ataxia

Youngsoo Kim[1,2], Seong Hun Kim[4], Kook Hwan Kim[5], Sujin Chae[3], Chanki Kim[7], Jeongjin Kim[1], Hee-Sup Shin[7], Myung-Shik Lee[5,6,*] and Daesoo Kim[1,*]

[1]Department of Biological Sciences, Korea Advanced Institute of Science and Technology (KAIST), 335 Gwahak-ro, Yuseong-gu, Daejeon 305-701, Republic of Korea, [2]Graduate School of Medical Science and Engineering, [3]KAIST Institute for BioCentury, KAIST, Daejeon 305-701, Republic of Korea, [4]Samsung Advanced Institute for Health Sciences and Technology, Sungkyunkwan University School of Medicine, Seoul 135-710, Republic of Korea, [5]Severans Biomedical Research Center Institute, [6]Department of Internal Medicine, Yonsei University College of Medicine, 50 Yonsei-ro Seodaemun-gu, Seoul 120-752, Republic of Korea and [7]Center for Cognition and Sociality, Institute for Basic Science (IBS), Daejeon, Republic of Korea

*To whom correspondence should be addressed. Tel: +82 42 350 2639; Fax: +82 42 350 5639; Email: daesoo@kaist.ac.kr (D. Kim)/Tel: +82 2 2228 0877; Email: mslee0923@yuhs.ac (M.-S. Lee)

Abstract

Really interesting new gene (RING) finger protein 170 (RNF170) is an E3 ubiquitin ligase known to mediate ubiquitination-dependent degradation of type-I inositol 1,4,5-trisphosphate receptors (ITPR1). It has recently been demonstrated that a point mutation of *RNF170* gene is linked with autosomal-dominant sensory ataxia (ADSA), which is characterized by an age-dependent increase of walking abnormalities, a rare genetic disorder reported in only two families. Although this mutant allele is known to be dominant, the functional identity thereof has not been clearly established. Here, we generated mice lacking *Rnf170* (*Rnf170*$^{-/-}$) to evaluate the effect of its loss of function *in vivo*. Remarkably, *Rnf170*$^{-/-}$ mice began to develop gait abnormalities in old age (12 months) in the form of asynchronous stepping between diagonal limb pairs with a fixed step sequence during locomotion, while age-matched wild-type mice showed stable gait patterns using several step sequence repertoires. As reported in ADSA patients, they also showed a reduced sensitivity for proprioception and thermal nociception. Protein blot analysis revealed that the amount of Itpr1 protein was significantly elevated in the cerebellum and spinal cord but intact in the cerebral cortex in *Rnf170*$^{-/-}$ mice. These results suggest that the loss of *Rnf170* gene function mediates ADSA-associated phenotypes and this gives insights on the cure of patients with ADSA and other age-dependent walking abnormalities.

Introduction

Walking is a fundamental motor function, and any problem therein significantly impairs the quality of life. Although the etiology is unknown, the capacity for elaborate walking coordination declines during the normal aging process, thereby increasing the risk of secondary accidents, especially in aged individuals (1,2). In various genetic and non-genetic motor disorders, patients develop gait problems as secondary symptoms that become more

Received: July 13, 2015. **Revised and Accepted:** September 29, 2015

severe with age (3–5). It is likely that aging negatively affects the rapid adaptation to sensory feedback during varied walking conditions (6,7). Therefore, identifying molecular targets responsible for this impaired adaptation may provide insight into age-dependent walking abnormalities.

RNF170 [symbol for the really interesting new gene (RING) finger protein 170 (human)] is an E3 ubiquitin ligase that mediates the ubiquitination-dependent degradation of proteins. A previous study demonstrated that the endoplasmic reticulum (ER) membrane-resident protein, inositol 1,4,5-triphosphate receptor type 1 (ITPR1), is a target of RNF170 (8). Because ITPR1 plays diverse cellular roles through mobilization of Ca^{2+} from the ER in response to external stimuli [for a review, see reference (9)], it has been speculated that RNF170 mediates various Ca^{2+}-dependent functions in neuronal and non-neuronal tissues [for a review, see reference (10)]. Despite identification of a relevant role at the molecular level, the *in vivo* functions of RNF170 have not been extensively explored.

A recent study reported that a missense mutation (595C>T) in exon 7 of the *RNF170* gene that causes an amino acid substitution (arginine → cysteine) is associated with autosomal-dominant sensory ataxia (ADSA, OMIM #608984), a rare hereditary form of ataxia (11). Patients with ADSA show a progressive loss of sensory feedback resulting in gait abnormality (11–13). When expressed in zebrafish, the human RNF170 mutant causes prenatal death with structural defects (11). Interestingly, however the human *RNF170* mutation does not affect the ubiquitination of activated ITPR1, an endogenous function of RNF170 (14). Based on these results, it has been thought that the age-dependent gait problem of human patients might be due to a gain-of-function of mutant RNF170 proteins, which is independent from endogenous RNF170 function. Addressing ADSA through therapeutic means depends on the confirmation of this hypothesis. To resolve this issue, it remains to be determined whether the mutant phenotype is also recapitulated or not when RNF170 protein is completely eliminated.

Results

Generation of knockout mice lacking Rnf170 protein

To examine the *in vivo* function of Rnf170, we produced an $Rnf170^{+/-}$ mouse line using strain 129-based embryonic stem cells (ESCs) containing a gene-trap vector targeting intron 2 located between exons 2 and 3 (OST104375, OmniBank; Fig. 1A). Heterozygous mice ($Rnf170^{+/-}$) were backcrossed with the C57BL/6 strain for at least six generations and intercrossed to produce F1 $Rnf170^{-/-}$ and $Rnf170^{+/+}$ (wild-type, WT) mice (Fig. 1B). Quantitative real-time reverse transcriptase-polymerase chain reaction (RT-PCR) analyses of representative tissues [brain, spinal cord, liver and brown adipose tissue (BAT)] revealed that $Rnf170^{-/-}$ mice lacked mRNA expression of this gene (brain, 0.001 ± 0.0005; spinal cord, 0.001 ± 0 in Fig. 1C; liver, 0.002 ± 0.0007; BAT, 0.0027 ± 0.0013 in Supplementary Material, Fig. S1B). These results suggest that despite the intronic insertion, the gene-trap vector efficiently terminates transcription of the *Rnf170* gene, as expected based on the vector design.

Normal growth and glucose metabolism in $Rnf170^{-/-}$ mice

Because Rnf170 mRNA is ubiquitously expressed in various neural and non-neural tissues (Supplementary Material, Fig. S1), we first investigated the general condition of $Rnf170^{-/-}$ mice. Growth curves, determined by measuring body weights between 5 and 17 weeks of age, were not significantly different between WT and $Rnf170^{-/-}$ mice (Fig. 1D). Because Rnf170 is known to be associated with Ca^{2+} signaling pathway (8,10), which mediates insulin secretion and various energy metabolism processes (15) [for a review, see reference (16)], we examined glucose metabolism. Measurements of blood glucose levels under random feeding conditions in 5- and 10-week-old mice revealed no significant differences between genotypes (Fig. 1E). Next, we tested glucose and insulin tolerance test to examine their response to hyper- and hypoglycemic conditions but found no significant differences between $Rnf170^{-/-}$ and WT mice (Fig. 1F and G). In addition, monitoring of survival rates in both WT and $Rnf170^{-/-}$ animals for 24 months after birth did not reveal any significant difference [$Rnf170^{-/-}$, $n = 12/15$ (80%); WT, $n = 12/15$ (80%)]. Collectively, these results support the unexpected conclusion that a loss of Rnf170 does not lead to any significant defects in postnatal development and overall body health.

Progressive gait abnormality in old $Rnf170^{-/-}$ mice

Because a mutation in *RNF170* gene leads to the progressive walking impairment in ADSA patients (11), we compared the motor capacity of $Rnf170^{-/-}$ mice with age-matched WT littermates at 3, 6 and 12 months of age. Interestingly, we found that only 12-month-old $Rnf170^{-/-}$ mice exhibited unstable walking compared with control mice (Supplementary Material, Video). To quantify the gait abnormality, we precisely compared the four-limb spatiotemporal stepping pattern during walking. First, we compared the degree of synchronization between diagonal limb couplets, which is known to increase during normal trotting (fast walking) (17,18). Whereas stepping of diagonal limb couplets during fast walking was synchronized in all other groups (Fig. 2A–C, D top), that of 12-month-old $Rnf170^{-/-}$ mice was remarkably asynchronous (Fig. 2D, bottom).

For quantitative analyses, inter-limb coupling was measured by calculating lag phases from the interval between onset times of each paw in a couplet contacting the floor (Fig. 2E, 'Materials and Methods'). If diagonal limbs move synchronously, the calculated value of inter-limb coupling is 0. The circular scatter plots shown in Figure 2(F–H) display the distribution of inter-limb coupling in each trial. Whereas WT mice and young $Rnf170^{-/-}$ mice showed a narrow distribution around a value of 0, 12-month-old $Rnf170^{-/-}$ mice showed a significantly more dispersed distribution (Fig. 2H, outer circle), which averaged 12.3% ± 1.5% compared with 2.8% ± 0.7% in WT mice (Fig. 2K). There were no significant differences among WT and 3- and 6-month-old $Rnf170^{-/-}$ groups (Fig. 2I and J). These results indicate that $Rnf170^{-/-}$ mice progressively develop asynchronous movements of diagonal couplets.

In contrast to diagonal limb pairs, homolateral (lateral) pairs are known to alternate during fast walking (17). When two limbs alternate perfectly, the inter-limb coupling value is 50% (i.e. in the middle of consecutive steps). We found that homolateral pairs showed a more dispersed lag phase in 12-month-old $Rnf170^{-/-}$ mice compared with those in WT mice (Supplementary Material, Fig. S2). Whereas WT mice showed a narrow distribution around a value of 50, 12-month-old $Rnf170^{-/-}$ mice exhibited a more dispersed distribution, averaging 12.5% ± 1.5% compared with 4.3% ± 0.5% in WT mice (Supplementary Material, Fig. S2B). Thus, homolateral coupling is also disrupted by the loss of Rnf170 protein at about 12 months of age.

The combination of paws contacting the ground, termed the support pattern, also reflects limb coordination. The

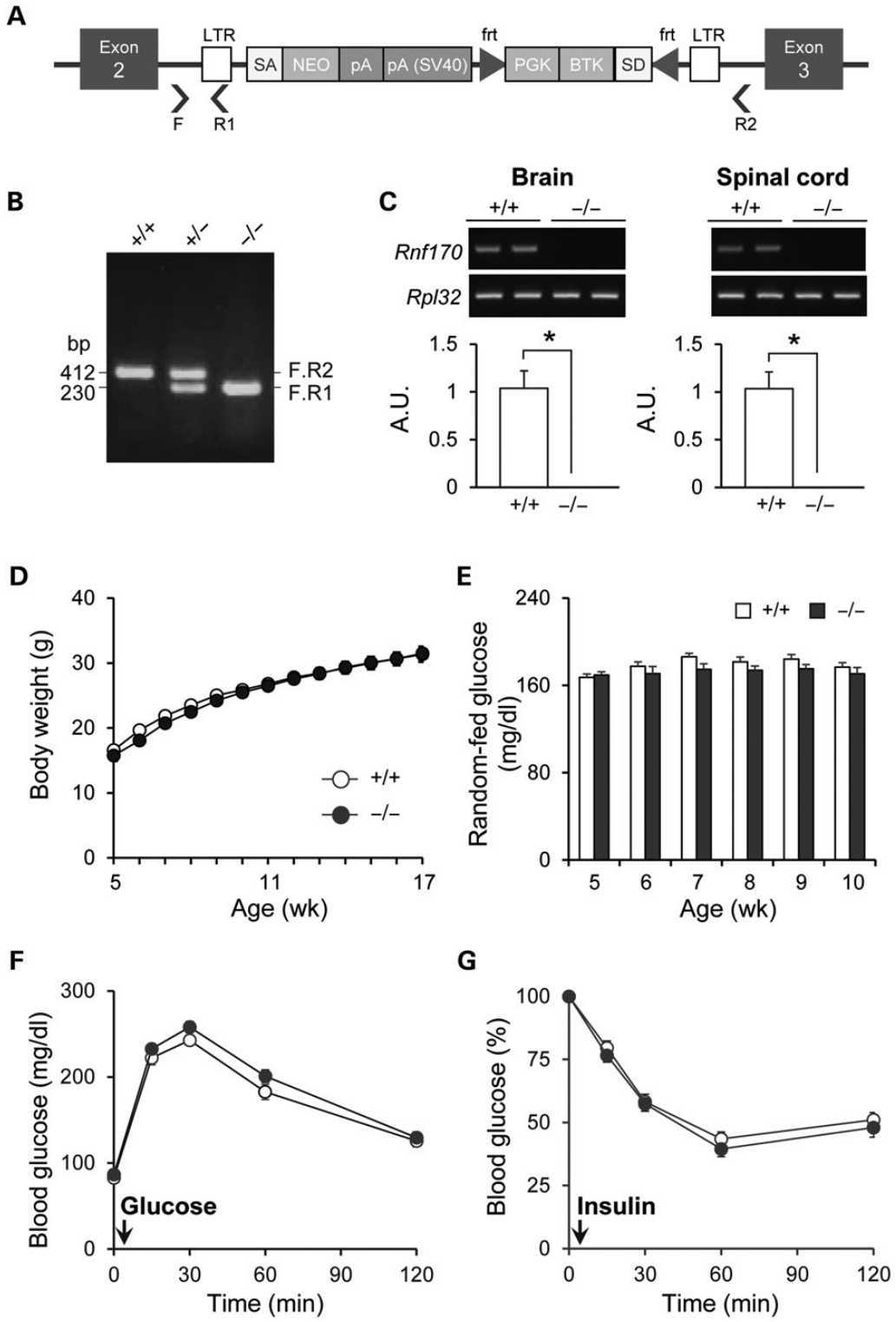

Figure 1. *Rnf170*$^{-/-}$ mice grow normally and exhibit normal metabolic function. (**A**) *Rnf170*$^{-/-}$ mice generated from an ESC line containing a gene-trap construct in intron 2. (**B**) The primers used in genomic DNA PCR (denoted by arrowheads in panel A). A PCR product obtained using F and R1 was detected in *Rnf170*$^{+/-}$ and *Rnf170*$^{-/-}$ mice. (**C**) Quantitative analysis of real-time RT-PCR was performed using brain samples from 25-months-old *Rnf170*$^{+/+}$ and *Rnf170*$^{-/-}$ mice ($n = 3$ each; *$P < 0.05$, *Rnf170*$^{+/+}$ versus *Rnf170*$^{-/-}$ mice; two-tailed unpaired *t*-test). (**D–G**) Growth and metabolic function parameters measured in *Rnf170*$^{+/+}$ and *Rnf170*$^{-/-}$ mice. Body weight (D) was not significantly different between *Rnf170*$^{+/+}$ ($n = 14$) and *Rnf170*$^{-/-}$ ($n = 15$) mice ($P = 0.648$, *Rnf170*$^{+/+}$ versus *Rnf170*$^{-/-}$ mice, two-way repeated measurement ANOVAs). Random-fed glucose level (E), measured at 5–10 weeks, was not significantly different between *Rnf170*$^{+/+}$ ($n = 14$) and *Rnf170*$^{-/-}$ ($n = 15$) mice ($P = 0.590$, $P = 0.342$, $P = 0.054$, $P = 0.131$, $P = 0.098$ and $P = 0.313$, at 5–10 weeks, respectively, two-tailed unpaired *t*-test). Glucose tolerance tests (F), performed at 5 months of age, showed no significant differences between *Rnf170*$^{+/+}$ ($n = 14$) and *Rnf170*$^{-/-}$ ($n = 15$) mice ($P = 0.148$, *Rnf170*$^{+/+}$ versus *Rnf170*$^{-/-}$ mice, two-way repeated-measures ANOVA). Insulin tolerance test results at 5 months (G) were also not significantly different between *Rnf170*$^{+/+}$ ($n = 12$) and *Rnf170*$^{-/-}$ ($n = 13$) mice ($P = 0.434$, *Rnf170*$^{+/+}$ versus *Rnf170*$^{-/-}$ mice, two-way repeated-measures ANOVA). Blood glucose level in insulin tolerance tests was calculated relative to the value at 0 min. Values are presented as mean ± SEM (error bars).

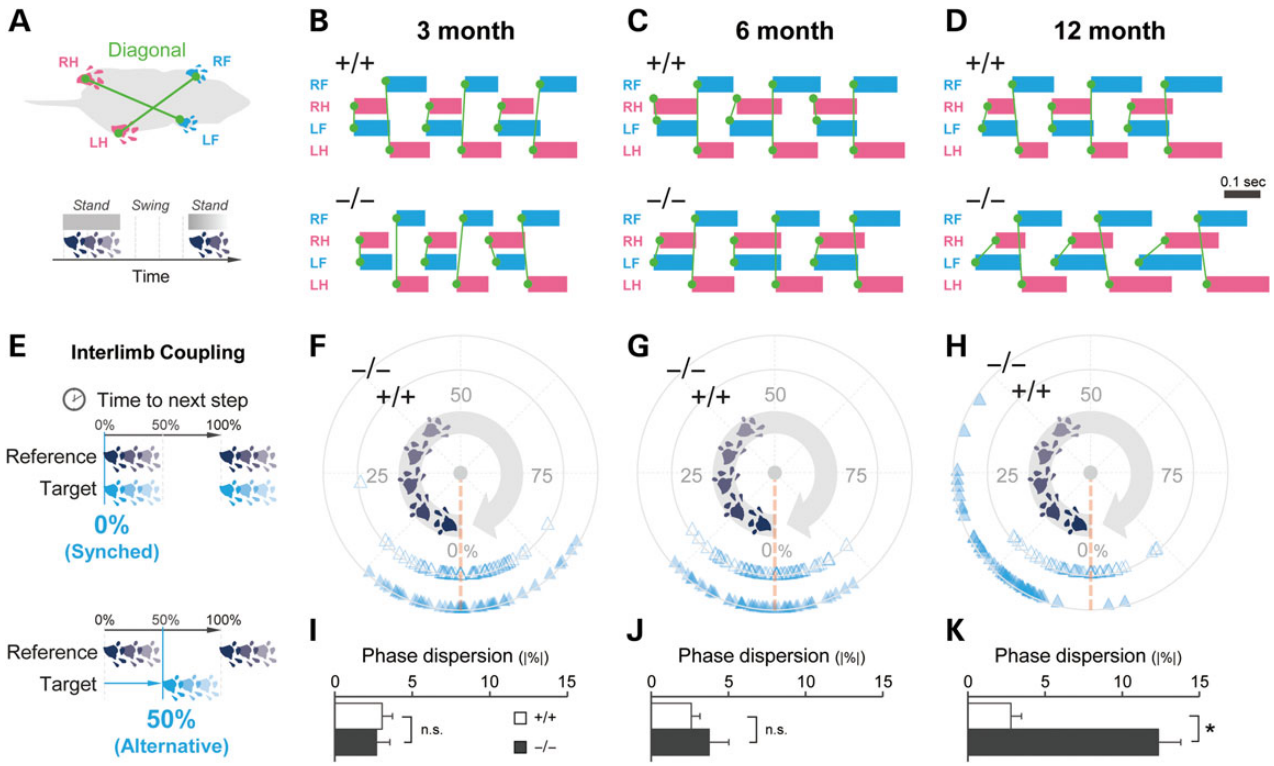

Figure 2. Old *Rnf170*$^{-/-}$ mice exhibit gait problems. (**A**) Temporal step patterns, measured to identify inter-limb coupled movements of diagonal pairs. Pink indicates hindlimbs and blue indicates forelimbs. Green lines indicate diagonal pairs. Standing time, in which a paw is in contact with the ground, is indicated as a filled bar. (**B–D**) Representative gate analysis trials performed on *Rnf170*$^{+/+}$ and *Rnf170*$^{-/-}$ mice at 3 months (B; $n = 7$ and 5, respectively), 6 months (C; $n = 7$ and 5, respectively) and 12 months (D; $n = 5$ for both genotypes). Color-coding is the same as that in (A). Inter-limb coupling was calculated from the lag phases between the onset of steps in paired paws. (**E**) The lag phases were calculated in a standardized value relative to the step cycle of reference paw, defined as 100%. Dark gray indicates reference paw and sky blue indicates target paw. In this method, 0% denotes completely synchronized movements of both paws. (**F–H**) Circular scatter plot showing the distribution of inter-limb coupling values at 3 months (F), 6 months (G) and 12 months (H). Color-coding is the same as that in (E). Red dotted line indicates the 0% point. (**I–K**) Average differences in inter-limb coupling, measured as phase dispersion, between *Rnf170*$^{+/+}$ and *Rnf170*$^{-/-}$ mice at 3 months (I), 6 months (J) and 12 months (K). Phase dispersion was significantly different between the two genotypes at 12 months (*$P = 0.0003$, two-tailed unpaired *t*-test), but was not significant (n.s.) at 3 months ($P = 0.432$, Mann–Whitney rank sum test) or 6 months ($P = 0.380$, two-tailed unpaired *t*-test). Values are presented as mean ± SEM (error bars). Abbreviations: RF, right forelimb; RH, right hindlimb; LF, left forelimb; LH, left hindlimb.

major pattern of support in mice is known as diagonal limb pairs (17,19); our results in WT mice and young *Rnf170*$^{-/-}$ mice were consistent with this dominant pattern (Supplementary Material, Fig. S3A). However, in keeping with the disrupted diagonal coupled movements (Fig. 2), the diagonal support pattern in 12-month-old *Rnf170*$^{-/-}$ mice (58.2% ± 2.1%) was significantly decreased compared with that of WT mice (75.6% ± 3.2%) (Supplementary Material, Fig. S3A and B). This result suggests that the loss of Rnf170 protein disrupts the inter-limb coupling and support pattern, which are important for walking stability.

Abnormal step sequence pattern in *Rnf170*$^{-/-}$ mice

Next, we analyzed the step sequence, which is known to be variable during fast walking in mice (17,19). There are six patterns of step sequence known in rodents (Fig. 3A, top): Ca, RF-LF-RH-LH; Cb, LF-RF-LH-RH; Aa, RF-RH-LF-LH; Ab, LF-RH-RF-LH; Ra, RF-LF-LH-RH and Rb, LF-RF-RH-LH. The upper case indicates three categories (cruciate, alternative and rotary), and the lower cases indicate horizontally reversed sequences. We found that only four patterns, Ca, Cb, Aa and Ab, were used in both genotypes, and frequencies of these four patterns in WT mice were similar to those described in a previous study (Fig. 3A) (17,19). Remarkably, 12-month-old *Rnf170*$^{-/-}$ mice showed a dominant increase in the Ab pattern (87.3% ± 5.4%) compared with WT mice (38.7% ± 5.8%), whereas 3- and 6-month-old *Rnf170*$^{-/-}$ mice showed a relative frequency similar to that of WT mice (Fig. 3A and B). These results indicate that an Rnf170 deficiency causes a restricted, modified step sequences only at about 12 months of age, establishing the characteristic pattern of support and step sequence associated with unstable walking in 12-month-old *Rnf170*$^{-/-}$ mice.

Normal motor learning and adaptation in *Rnf170*$^{-/-}$ mice

To confirm that the gait abnormalities in *Rnf170*$^{-/-}$ mice are determined as described above (Figs 2, 3 and Supplementary Material, Figs S2 and S3) and are not attributable to other parameters associated with walking performance, we examined averaged speed, stride length (distance) and step cycle (time). Although previous studies describe that inter-limb coupling changes as a function of walking speed (17,18), old *Rnf170*$^{-/-}$ mice showed no significant differences in walking speed, stride length and cycles compared with WT mice (Fig. 4A). To determine whether abnormal walking is associated with other motor dysfunctions, as previously described (20–22), we tested motor learning and adaptation in *Rnf170*$^{-/-}$ mice, performing rotarod and beam-walking tests with *Rnf170*$^{-/-}$ and WT mice at 15–16 months of age. There was no significant difference in the latency to fall in

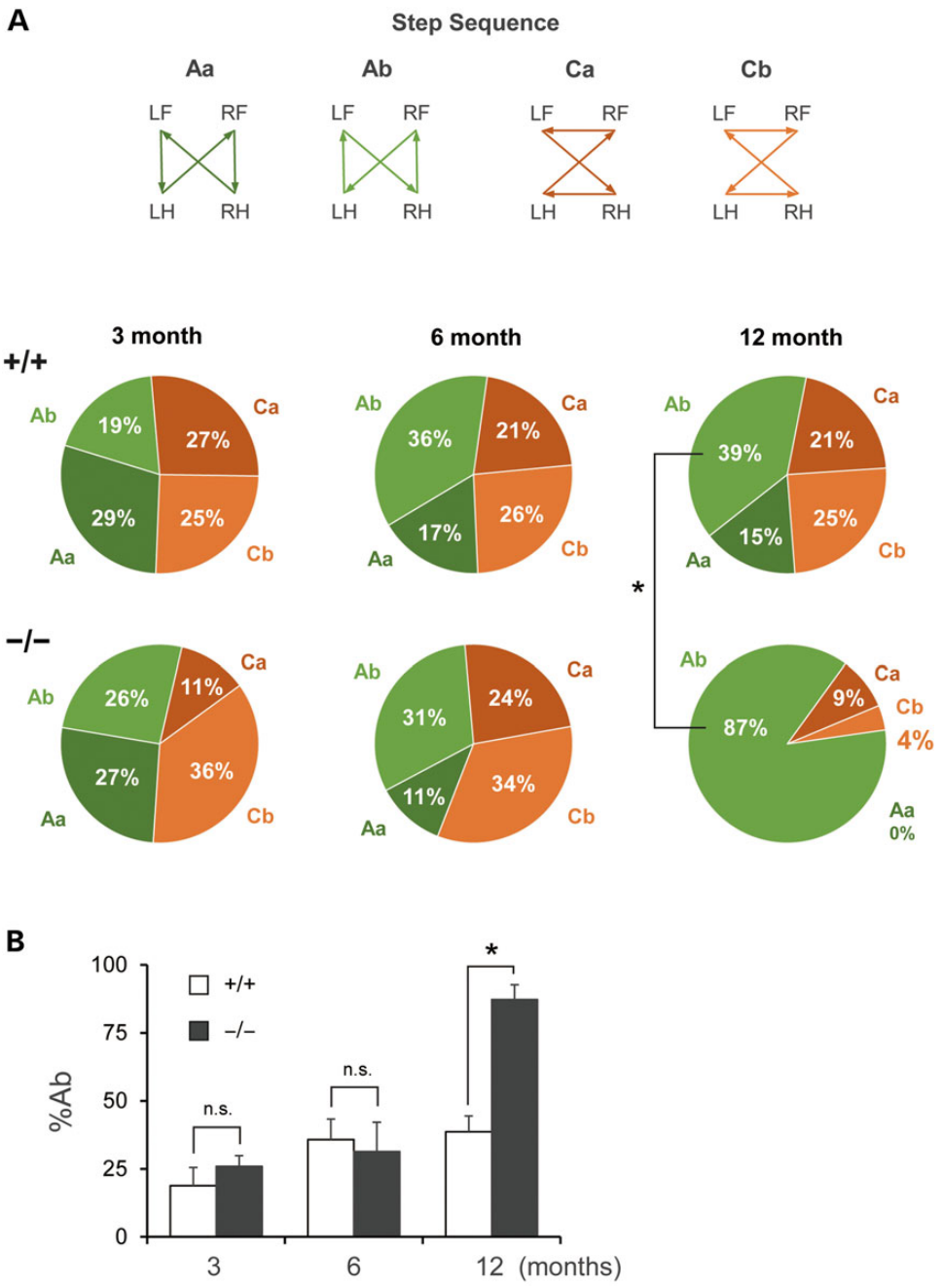

Figure 3. Restricted step sequence in old *Rnf170*$^{-/-}$ mice. (**A**) Step sequences, sorted into four patterns, are presented as a pie graph showing the relative frequency of each pattern during the experiment. Dark green, alternative a (Aa) pattern; light green, alternative b (Ab); dark orange, cruciate a (Ca); light orange, cruciate b (Cb). (**B**) Bar graph showing the average relative frequency of each Ab sequence for *Rnf170*$^{+/+}$ and *Rnf170*$^{-/-}$ mice at 3, 6 and 12 months of age. Step sequences were significantly different at 12 months (*$P = 0.00028$, two-tailed unpaired *t*-test), but were not significant (n.s.) at 3 months ($P = 0.430$, two-tailed unpaired *t*-test) or 6 months ($P = 0.736$, two-tailed unpaired *t*-test). The same samples used in Figures 2 and 3 were employed in the analysis. Values are presented as mean ± SEM. (error bars).

an accelerating rod test or in activities on the beam (Fig. 4B and C). These results suggest that the gait abnormality of the *Rnf170*$^{-/-}$ mice is not a secondary effect but specifically associated with the mechanism that modulates inter-limb coupling and step sequences.

Sensory dysfunctions in *Rnf170*$^{-/-}$ mice

Given that a key feature of sensory ataxia is the loss of proprioception and other sensory faculties concerning pain, temperature and vibration, which becomes more distinct in aged patients (11–13), we tested sensory function in 24–26-month-old *Rnf170*$^{-/-}$ mice (Supplementary Material, Fig. S4A–C), which showed normal body weights and fasting glucose levels compared with WT mice (Supplementary Material, Fig. S4D and E). First, we performed the H-reflex test, in which electrical stimulation of muscle fibers directly induces muscular activity (M-wave) and delayed muscular activity depending on activation of sensory neurons in spinal reflex circuits, called an H-wave (22,23). Proprioceptive sensory function was assessed by the ratio of amplitude between maximum

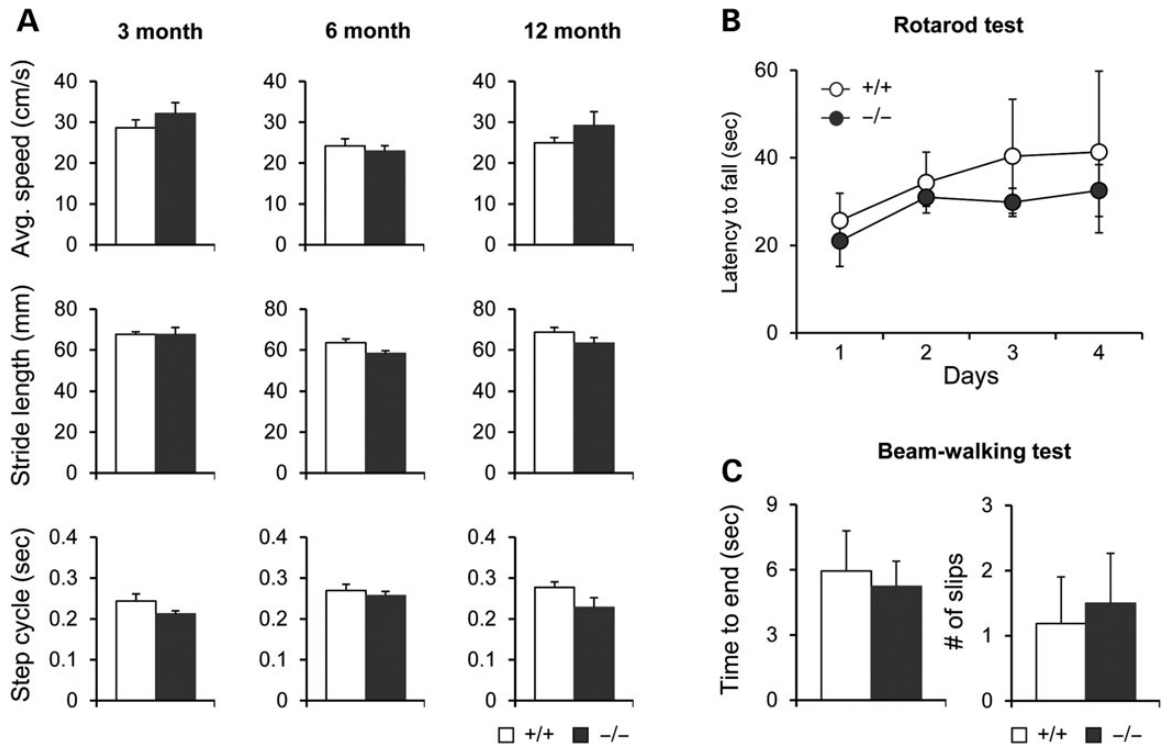

Figure 4. *Rnf170*$^{-/-}$ mice have no significant defects in other motor functions. (**A**) Parameters indicating general motor performance of *Rnf170*$^{+/+}$ and *Rnf170*$^{-/-}$ mice were measured by gait analysis at 3, 6 and 12 months using the same samples employed in Figures 2–4. Bar graphs show that general motor performance was not significantly different between genotypes (two-tailed unpaired *t*-test), measured as average speed ($P = 0.300$, $P = 0.606$, and $P = 0.285$ at 3, 6 and 12 months, respectively), stride length ($P = 0.966$, $P = 0.054$ and $P = 0.150$ at 3, 6 and 12 months, respectively) and step cycles ($P = 0.197$, $P = 0.560$ and $P = 0.110$ at 3, 6 and 12 months, respectively). (**B**) Rotarod tests were performed on four consecutive days. Latency to fall from the accelerating rod, measured at 15–16 months of age, was not significantly different between *Rnf170*$^{+/+}$ ($n = 4$) and *Rnf170*$^{-/-}$ ($n = 4$) mice ($P = 0.575$, two-way repeated-measures ANOVA). (**C**) Beam-walking tests were performed using the same mice as in (B). After training, mice that crossed the beam without hesitation were used for the analysis (*Rnf170*$^{+/+}$, $n = 4$; *Rnf170*$^{-/-}$, $n = 3$). There were no significant differences between genotypes with respect to time to cross the beam ($P = 0.78$, two-tailed unpaired *t*-test) or average number of slips during the cross ($P = 0.78$, two-tailed unpaired *t*-test). Values are presented as mean ± SEM (error bars).

H- and M-waves (H/M ratio) (24). Remarkably, we found that *Rnf170*$^{-/-}$ mice showed significantly lower H/M ratios (11.0% ± 5.4%) compared with WT mice (31.2% ± 5.7%; Fig. 5A). Furthermore, we measured grip strength, which is sensitive to the loss of proprioception (22), and found significantly lower values in *Rnf170*$^{-/-}$ mice (1.7 ± 0.1 N) compared with WT mice (2.4 ± 0.1 N; Fig. 5B). These results collectively imply that *Rnf170*$^{-/-}$ mice have problems with proprioceptive function, which may lead to the gait abnormalities observed. Second, we compared thermal nociception using the hot plate test and found that the latency to pain response was significantly longer in *Rnf170*$^{-/-}$ mice (14.9 ± 1.1 s) compared with WT mice (11.3 ± 0.8 s; Fig. 5C). Third, because patients are known to be more dependent on visual cues during locomotion to compensate for their walking instability, their symptoms become more severe under dark conditions (25). Therefore, we investigated whether the gait abnormalities in *Rnf170*$^{-/-}$ mice are associated with visual cues. We developed a test paradigm in which the degree of waddling was measured by tracking a visible marker attached to the proximal part of the mouse's tail under both light and dark conditions (Fig. 5D, left; see 'Materials and Methods'). *Rnf170*$^{-/-}$ mice showed more waddling than WT mice (2.0 ± 0.3 cm versus 0.8 ± 0.1 cm; two-tailed unpaired *t*-test, $P = 0.009$), and this became more acute under dark conditions (2.4 ± 0.3 cm) (Fig. 5D and E). These results suggest that the loss of Rnf170 function is also involved in ADSA-like sensory dysfunction.

Increased Itpr1 proteins in *Rnf170*$^{-/-}$ mice

Given that dysregulation of intracellular Ca^{2+} concentration ($[Ca^{2+}]_i$) has been implicated as a molecular mechanism of ataxia (26–28) and that RNF170 mediates ubiquitination-dependent degradation of ITPR1 that in turn controls $[Ca^{2+}]_i$ (8), ITPR1 can be a relevant target for the mechanism of abnormalities found in ADSA patients with a mutation in *RNF170* gene. However, this hypothesis remains unproved because previous studies have shown that lymphoblast cells obtained from ADSA patients with RNF170 mutation show normal amounts of ITPR1 proteins (14), suggesting the possibility that phenotypes of ADSA are independent from the endogenous role of RNF170. To determine this point, we checked whether the expression level of Itpr1 protein is increased in neuronal tissues obtained from the cerebral cortex, cerebellum and spinal cord of old *Rnf170*$^{-/-}$ mice. Indeed, they showed a significant increase of Itpr1 proteins in the cerebellum and spinal cord (cerebellum, 1.44 ± 0.12 a.u.; spinal cord, 3.65 ± 0.53 a.u.) compared with WT mice (cerebellum, 1.00 ± 0.12 a.u.; spinal cord, 1.00 ± 0.12 a.u.; Fig. 6A and B). In contrast, such an increase in Itrp1 was not observed in the cerebral cortex (*Rnf170*$^{-/-}$, 1.09 ± 0.12 a.u.; WT, 1.00 ± 0.15 a.u.; Fig. 6C). These results suggest that RNF170 plays a critical role in the regulation of ITPR1 by acting on particular neural tissues associated with motor coordination.

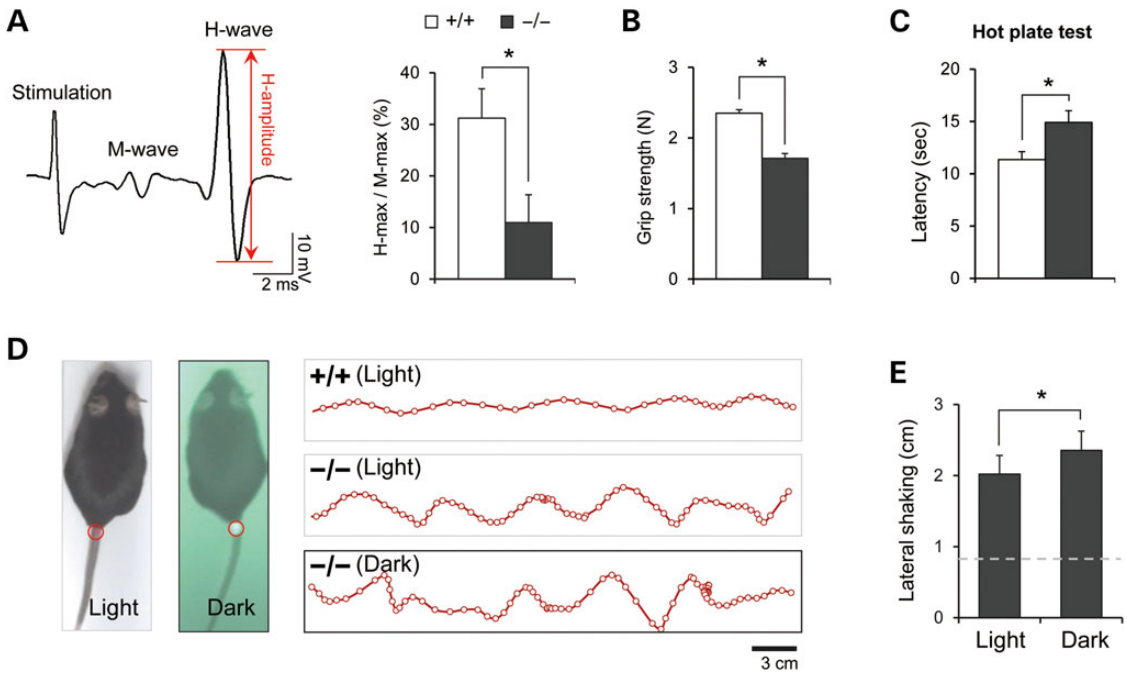

Figure 5. Sensory dysfunctions in old *Rnf170*$^{-/-}$ mice. (**A**) Representative trace shows successfully induced H-wave by electrical stimulation. Smaller M-wave can be discriminated from the H-wave. Bar graph shows the H/M ratio calculated from the maximum amplitude of H- and M-wave. There was significant differences between *Rnf170*$^{-/-}$ and *Rnf170*$^{+/+}$ mice ($n = 4$ each, $^*P = 0.0423$, two-tailed unpaired *t*-test). (**B**) Grip strength was measured as the maximum values until release. There was significant differences between *Rnf170*$^{-/-}$ and *Rnf170*$^{+/+}$ mice ($n = 7$ each, $^*P < 0.0001$, two-tailed unpaired *t*-test). (**C**) Hot plate test was performed to measure the latency for the nociceptive reaction by heat. The latency was significantly different between *Rnf170*$^{-/-}$ ($n = 7$) and *Rnf170*$^{+/+}$ ($n = 8$) mice ($^*P = 0.0181$, two-tailed unpaired *t*-test). (**D**) Snapshots shows the experimental procedures used to track body movements of mice both in light and dark conditions. The red circle indicates the same marker attached onto the mouse's tail. This marker was detected with a color-based filter in the light condition, and a brightness-based filter in the dark condition. Traces show the representative result of body movements during walking in each condition. Dots on the trace indicate the location of the marker in each video frame. (**E**) The instability intensity was measured by averaging the values for lateral body movement in a trial. There were significant differences between light and dark conditions in 24–26-month-old *Rnf170*$^{-/-}$ mice ($n = 5$, $^*P = 0.0165$, two-tailed paired *t*-test). The mean value from WT littermates in the light condition ($n = 6$) is indicated as a gray dotted line. Values are presented as mean ± SEM (error bars).

Discussion

The identification of gene mutations in patients provides insight into physiological and pathophysiological roles of the target gene. ADSA is a dominant genetic disorder characterized by age-dependent gait abnormalities and is the only reported human disease directly linked to a point mutation in the *RNF170* gene (11–13). The simplest explanation for this linkage would be that the mutant RNF170 possesses new functions (neomorph), such as harmful effects on motor coordination not related to the endogenous role of RNF170. However, this is unlikely because *Rnf170*$^{-/-}$ mice showed a similar ADSA-like phenotype, suggesting that Rnf170 protein is necessary for the regulation of age-dependent gait via association with sensory function, and that mutation of the *Rnf170* gene may impair the endogenous function of the corresponding protein, thus causing sensory ataxia.

Several possible mechanisms could account for the effects of this mutation based on our findings. First, the mutation could cause a loss of function because the dosage of the normal protein is insufficient for normal activity in a heterozygous state (haploinsufficiency). A recent study (14) reported that RNF170 protein expression is reduced (27%) in lymphoblast cell lines obtained from ADSA patients, which is consistent with our finding that *Rnf170*$^{-/-}$ mice have an ADSA-like phenotype. Although apparently conflicting results have been obtained from RNF170 measurements in spinal cord samples from ADSA patients, this study did not include quantitative analyses (11). Second, mutant RNF170 proteins could interfere with normal protein function through a dominant negative mechanism (antimorph). In line with this possibility, many RING-domain E3s are known to function through dimerization [for a review, see (29)]. It remains to be determined whether RNF170 functions through dimerization, which is linked to the question of whether the mutation affects protein–protein interactions. Finally, our results strongly suggest that an effective treatment for ADSA would be toward increasing RNF170 or compensating for its loss of function.

Through behavioral analyses, we also revealed that old *Rnf170*$^{-/-}$ mice develop gait abnormalities without any other motor dysfunctions (Figs 2–4), implying that human ADSA involves a specific alteration in the mechanism of limb coordination and further suggesting that *Rnf170*$^{-/-}$ mice are a robust model for the study of step sequence coordination. Interestingly, many animal models display both motor dysfunctions and walking abnormalities (20–22), raising the question of why *Rnf170*$^{-/-}$ mice show normal function in general motor tests until 16 months of age. It has been reported that despite significant motor coordination difficulties, ADSA patients adapt well to their body conditions using compensatory walking (30) or reaching (31) strategies facilitated through rehabilitation. Further studies on this adaptive mechanism in *Rnf170*$^{-/-}$ mice should provide insight into the possibility of treating ADSA through rehabilitation.

A high-speed visualization system used to precisely analyze the gait of *Rnf170*$^{-/-}$ mice yielded a number of mechanistic insights into age-dependent gait control. First, the coupled movement of diagonal couplets was disrupted in the gait of 12-month-old *Rnf170*$^{-/-}$ mice (Fig. 2 and Supplementary Material, Fig. S3).

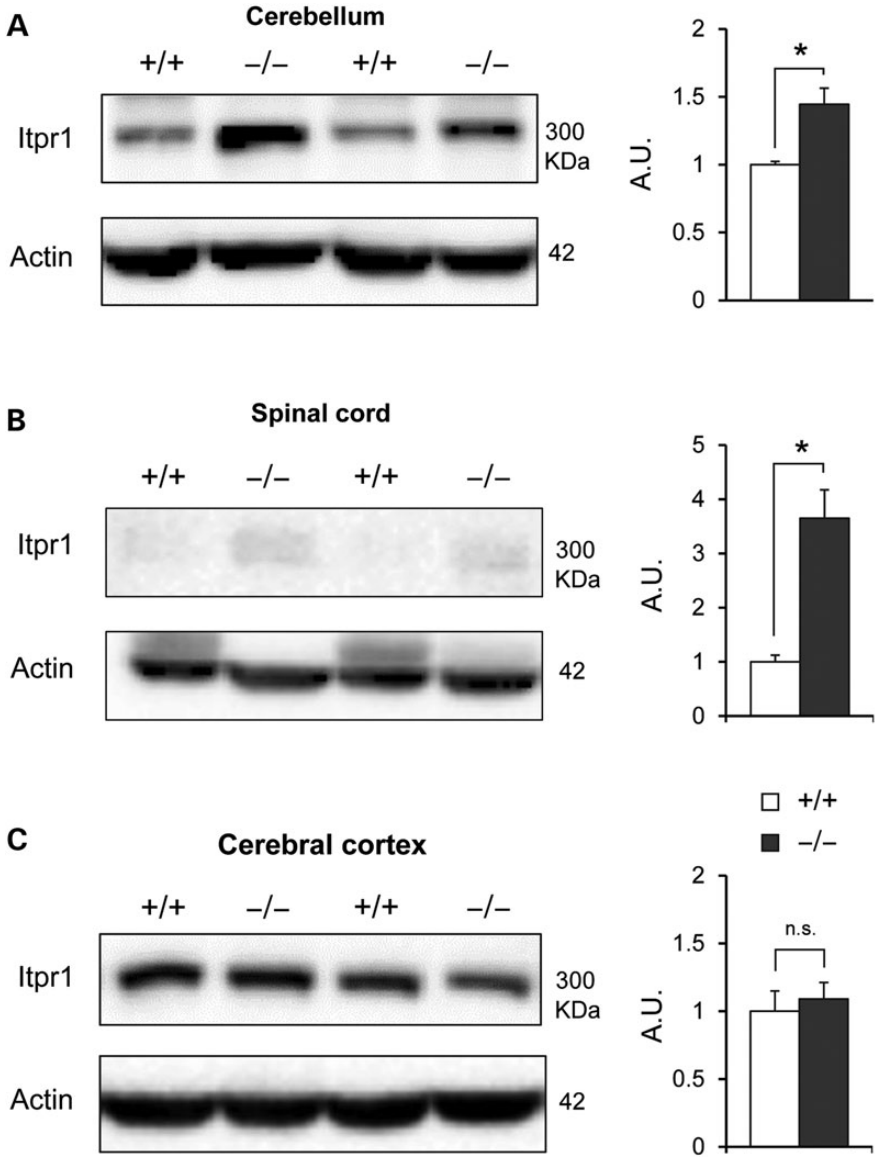

Figure 6. Increased Itpr1 expression in specific nervous tissues of old *Rnf170*$^{-/-}$ mice. (**A–C**) Quantitative analysis of Itpr1 protein expression was performed with western immunoblotting with tissues of the cerebellum (A; *P = 0.0213), spinal cord (B; *P = 0.0082) and cerebral cortex (C; P = 0.662) from the 24–26-month-old *Rnf170*$^{+/+}$ and *Rnf170*$^{-/-}$ mice ($n = 3$ each; *Rnf170*$^{+/+}$ versus *Rnf170*$^{-/-}$ mice; two-tailed unpaired *t*-test). Values are presented as mean ± SEM (error bars).

Diagonal couplet synchronization is important for maintaining balance during movement in most animals and helps maintain stability and reduce energy expenditure (32–34). Second, we found that old *Rnf170*$^{-/-}$ mice showed a restricted pattern of step sequences during walking (Fig. 3). Given that walking consists of sequential limb movements and that flexible modification of the sequence is essential for stable walking under various conditions, the significance of the modified limb sequence is not restricted to walking, but can be extended to complex movements that are modified according to variable environmental conditions. Taken together, our findings indicate that the *Rnf170*$^{-/-}$ mouse has features of walking disabilities like those found in elderly ADSA patients.

The spinal cord has long been considered as a key regulator of rhythmic locomotion (35,36), a notion supported by previous reports that the ablation of specific types of neurons in the spinal cord induces an altered gait, such as hopping (37,38). Studies on ADSA and our results suggest that this spinal mechanism of walking coordination may require sensory feedback. ADSA patients exhibit progressive loss of sensory functions (11–13) and pathological changes in the dorsal column of the spinal cord through which sensory information is relayed (39). Deficiency of proprioception due to problems in the spinal cord is known to cause abnormal inter-limb coupling (21) as seen in *Rnf170*$^{-/-}$ mice. Therefore, it remains a relevant issue as to how RNF170 mediates sensorimotor coupling in the spinal cord. Anatomical and physiological comparisons of spinal sensory and motor circuits in *Rnf170*$^{-/-}$ and WT mice, and the production of spinal cord specific *Rnf170* knockout models will give answers.

At the molecular level, understanding the function of RNF170 has heuristic value in answering how E3 ubiquitin ligases regulate neuronal functions that control motor activity. Ubiquitination is an essential mechanism in the post-translational modification of proteins, and this process requires a cascade of ubiquitin-activating (E1), ubiquitin-conjugating (E2) and ubiquitin-ligating (E3) enzymes. For target-specific ubiquitination, E3s

play a key role in recognizing target proteins and transferring the ubiquitin molecule, which is conjugated by E2s. Despite the significance of E3s, the roles of individual E3s *in vivo* have been defined in only a few cases (10). Here we identify the contribution of RNF170, among E3s with identified target substrates, in the modulation of ITPR1 *in vivo* (Fig. 6). Because ITPR1 is involved in intracellular Ca^{2+} regulation, any compensation of this function may lead to beneficial therapeutic effects on ADSA. Revealing the precise connection between the loss of RNF170 function and Ca^{2+} regulation through ITPR1 will provide critical information, which can be a great step forward in the development of drugs treating age-dependent gait problems.

Materials and Methods

Animal care

Animal care and experiments were conducted in accordance with the guidelines of the Institutional Animal Care and Use Committee of Sungkyunkwan University School of Medicine and Korea Advanced Institute of Science and Technology (KAIST). All mice were maintained on a 12:12 h light:dark cycle (light cycle beginning at 6:00 AM) at a temperature of 23°C. Food and water were supplied *ad libitum*. All animal experiments employed male mice.

Generation of *Rnf170*$^{-/-}$ mice

Rnf170$^{-/-}$ mice were generated using a gene-trap method. The 129/SvEv-derived ESC line OST104375 containing the gene-trap vector VICTR48 was purchased from Texas A&M Institute for Genomic Medicine. The gene-trap cassette was inserted into intron 2 located downstream of exon 2 containing the ATG translation-initiation codon. Chimeras were backcrossed to the C57BL/6 background for at least six to seven additional generations. Genotypes of mice were determined by polymerase chain reaction (PCR) using the following primers: 5′-ACT GTA TCT GAA GCC TTC TCA A-3′ (forward, both WT and *Rnf170*$^{-/-}$ mice), 5′-TAA ACC AGT AAT GCT ACA CAG G-3′ (reverse, WT) and 5′-ATA AAC CCT CTT GCA GTT GCA TC-3′ (reverse, *Rnf170*$^{-/-}$). The PCR fragment sizes for WT and *Rnf170*$^{-/-}$ mice were 412 and 230 bp, respectively.

RNA isolation and analysis

Total RNA from various tissues was isolated using TRIzol (Invitrogen, USA) and purified using an RNA clean up kit (GeneAll Biotechnology, South Korea) according to the manufacturer's instructions. cDNA was synthesized from 2 μg of total RNA by incubating with Moloney Murine Leukemia Virus reverse transcriptase (Promega, USA) and oligo(T) primers at 42°C for 1 h. An aliquot (1/30 vol) of cDNA was then amplified by PCR using the following primer pairs: RNF170, 5′-ATT GGC GTT TCC AAG ACA AC-3′ (forward) and 5′-ATA CAG GAG AGT AGC GGT CA-3′ (reverse), fragment size 200 bp; Rpl32, 5′-CAG TCA GAC CGA TAT GTG AA-3′ (forward) and 5′-TAG AGG ACA CAT TGT GAG CA-3′ (reverse), fragment size 265 bp. Real-time reverse transcription (RT)-PCR was conducted using SYBR Green Master Mix (Takara, Japan) in an ABI Prism 7000 system (Applied Biosystems, USA). Relative expression values were normalized to Rpl32 mRNA levels.

Western immunoblotting

Mouse brain parts (cerebellum, spinal cord and cerebral cortex) were harvested and snap frozen in LN2 and stored at −70°C deep freezer until used. Each brain tissue was homogenized with T-Per buffer (Tissue protein extraction buffer, #78510; Thermo Scientific, USA) containing 1× Protease inhibitor cocktail (cOmplete, EDTA-free, #11 873 580 001; Roche Diagnostics, USA) and 1× Phosphatase inhibitor cocktail (PhosSTOP, #04 906 837 001; Roche Diagnostics, USA). Lysates were incubated on ice for 1 h with frequent vortexing, and supernatant was collected by centrifugation at 13 000 rpm for 20 min at 4°C. The 50 μg of total protein was incubated at 37°C for 30 min prior to subject to 6% SDS-PAGE gels for Itpr1 and 10% gels for β-actin. Itpr1 was detected with anti-Itpr1 (IP3 Receptor 1(D53A5), #8568; Cell Signaling Technology, USA) and β-actin with anti-β-actin antibody (sc47778; Santa Cruz Biotechnology, USA). The proteins were visualized with the Super-Signal West Pico System (Thermo Scientific, USA).

Glucose tolerance and insulin tolerance tests

Glucose tolerance tests were performed on overnight-fasted mice following intraperitoneal injection of glucose (1 g/kg body mass). Insulin tolerance tests were conducted in 6 h-fasted mice following intraperitoneal injection of insulin (1 U/kg body mass). Blood glucose levels were measured using an Accu-Chek glucometer (Roche, Swiss).

Gait analysis

In-depth gait analyses were performed using the Catwalk apparatus (Noldus, Netherlands) containing a glass plate with internally reflecting light rays. The paws of mice were detected as reflected light, recorded with a high-speed camera oriented downward. During experiments, mice were allowed 30–60 min to freely explore the walkway, both ends of which were blocked with steel grids. Because mice were not habituated to the experimental environment, they exhibited the innate property of preferring the end of the walkway and rapidly crossed the runway. For data analysis, five to seven trials in which mice crossed the walkway without hesitation at a constant speed were used for each mouse. At least three step cycles were contained in a trial sample. All experiments and data analysis were performed in a blinded manner. Inter-limb coupling (Fig. 2 and Supplementary Material, Fig. S2) was calculated by measuring the onset of floor contact for each paw. Lag phases were calculated as the phase of the target paw toward the step cycle relative to the reference paw (as a percentage), where 0% indicates perfectly synchronized movement and 50% corresponds to perfectly alternating movement. To avoid repeated calculation with the same pair, the reference paw is always one of the front paw within diagonal and ipsilateral pair, and the left paw within girdle pair. This parameter is automatically calculated in Catwalk software as Phase Dispersions with circular statistics. In application, a value of 0 is equivalent to a value of 100, because phase lag is a circular variable. Support pattern (Supplementary Material, Fig. S3) is the relative duration of all combinations of paws that simultaneously contact the floor. Support patterns involving combinations of paw pairs (our focus) included diagonal pair (RF-LH or LF-RH), lateral pair (RF-RH or LF-LH) and girdle pair (RF-LF or RH-LH); other support patterns included zero paws, a single paw, three paws and four paws. Step sequence (Fig. 3) is the order in which the paws are placed on the floor. There are six possible sequence patterns in a quadrupedal gait; however, mice commonly use only four during walking, as confirmed by our results.

Rotarod test

Rotarod tests (Model 47600; Ugo Basile, Italy) were performed on four consecutive days. Mice were positioned on a rod rotating at

4 rpm; after 10 s, the rod was accelerated to 40 rpm at a rate of 20 rpm/min. The latency to fall, determined from 3 trials/day for each mouse, was measured after the initiation of acceleration. The experiment and analysis were performed in a blinded manner.

Beam-walking test

Beam-walking tests were performed using an acrylic beam 3 cm wide by 1 m in length elevated 50 cm above the floor. Evaluations were performed 1 day after training mice to cross the beam. Two trials in which the mice did not stay on the beam were analyzed per mouse per day; slips were counted by two individual investigators. Experiments and analyses were performed in a blinded manner.

Walking stability test both in the light and dark

The experiment was performed in the corridor used in the Catwalk experiments. The intensity of light was 70–80 lux (measured with TM-204 light meter; Tenmars Electronics Co., Taiwan) in the light condition, while all light sources were switched off in the dark condition. To control for any differences in detection quality under the light and dark conditions, we attached a circular light reflective marker on the proximal part of the mouse's tail. All footage was recorded with the same device (digital camcorder, Sony, Japan), with the infrared (IR) filter switched on for dark conditions. We fabricated the red-colored marker with retroreflective tape (#7610; 3M Co., USA), an effective reflector of IR light. This property enabled the marker to be detected as a bright point in IR-filtered video frames, and as a red-colored point in lit conditions. Video tracking was performed at the rate of 30 frames/s using Ethovision XT 8.5 software (Noldus, Netherlands). To compute the intensity of gait instability, the peak-to-peak amplitudes of lateral movements for each trial were obtained with Matlab software (Mathworks, USA). To exclude subtle movements not directly related to walking instability, only the top 33% values were used.

H-reflex test

H-reflex tests were performed with a protocol modified from previous studies (22,23). In detail, mice were anesthetized with an i.p. injection of Ketamine (100 mg/kg) and Xylazine (10 mg/kg) cocktail in phosphate-buffered solution (PBS). Additional injection with a 25% dose was administered when the mice showed any whisker tremor or body movements. After the limbs of the mice were fixed with paper tape, EMG signals were measured with a transcutaneously placed pair of tungsten electrodes (Cat no. 796500; A-M systems Inc., USA) connected to a signal amplifier (Model 9; Grass Instrument Co., USA). Signals were acquired with a digital acquisition system (Digidata 1322A; Molecular Devices LLC, USA) and pClamp software (Molecular Devices LLC, USA). Recorded signals were filtered in the frequency range of 0.1–1 kHz. The stimulation electrode was inserted into nerve bundles including the sciatic nerve and electrically stimulated with a stimulation isolator (World Precision Instruments, Inc., USA), controlled to generate 0.2 ms square-shaped pulses at 0.2 Hz. The stimulation intensity was sequentially increased by 0.05 mA, enabling us to distinguish between H-wave and M-wave peaks. Data analysis was performed using the pClamp software.

Grip strength test

To measure grip strength, the subject mouse was positioned on a mesh connected with a force meter (NK-20 model; Japan Instrumentation System Co., Japan). After the mouse grasped the mesh, its tail was smoothly pulled until it released its grip. Readings made on the meter were filmed with a camcorder, and the resulting video file was analyzed to determine the maximum strength of the mouse's grip. Three trials were performed on each mouse at 30 s intervals, and the averaged value of grip strength was used in analysis. Experiments and analyses were performed in a blinded manner.

Hot plate test

The hot plate test was performed with a hot plate analgesia meter (Model 39; IITC Life Science Inc., USA) set at 52.5°C. After mice were put into a bottomless acrylic cylinder located on the plate, their latency to nociceptive reaction was determined via video analysis. Behaviors defining nociceptive reaction included hind paw shaking, hind paw licking or jumping. All trails were performed by two different investigators and confirmed with video analysis. Experiments and analyses were performed in a blinded manner.

Supplementary Material

Supplementary Material is available at *HMG* online.

Acknowledgements

We thank Jeonghoon Woo and Ah Hyung Park (Department of Biological Sciences, KAIST) for advice on gait analysis, and Geunhong Park (Department of Biological Sciences, KAIST) for English editing.

Conflict of Interest statement. The authors of this study have no competing financial interests.

Funding

This work was supported by the National Research Foundation of Korea (NRF) funded by the Ministry of Science, ICT and future Planning [2011-0028772 (National Leading Research Laboratory Program) to D.K., K21004000003-12A0500-00310 (Global Research Laboratory Program) to M.-S.L., 2011-0031955 (Intelligent Synthetic Biology Center of Global Frontier Project) to S.C.].

References

1. Wilson, R.S., Schneider, J.A., Beckett, L.A., Evans, D.A. and Bennett, D.A. (2002) Progression of gait disorder and rigidity and risk of death in older persons. *Neurology*, **58**, 1815–1819.
2. Alexander, N.B. (1996) Gait disorders in older adults. *J. Am. Geriatr. Soc.*, **44**, 434–451.
3. Bird, T.D. (1998) Hereditary ataxia overview. In Pagon, R.A., Adam, M.P., Ardinger, H.H., Wallace, S.E., Amemiya, A., Bean, L.J.H., Bird, T.D., Fong, C.T., Smith, R.J.H. and Stephens, K. (eds), In *GeneReviews(R)* [Internet]. University of Washington, Seattle, WA, http://www.ncbi.nlm.nih.gov/books/NBK1138.
4. Hadjivassiliou, M., Grunewald, R., Sharrack, B., Sanders, D., Lobo, A., Williamson, C., Woodroofe, N., Wood, N. and Davies-Jones, A. (2003) Gluten ataxia in perspective: epidemiology, genetic susceptibility and clinical characteristics. *Brain*, **126**, 685–691.
5. Krawetz, P. and Nance, P. (1996) Gait analysis of spinal cord injured subjects: effects of injury level and spasticity. *Arch. Phys. Med. Rehabil.*, **77**, 635–638.

6. Van Emmerik, R.E., McDermott, W.J., Haddad, J.M. and Van Wegen, E.E. (2005) Age-related changes in upper body adaptation to walking speed in human locomotion. *Gait Posture*, **22**, 233–239.
7. Priest, A.W., Salamon, K.B. and Hollman, J.H. (2008) Age-related differences in dual task walking: a cross sectional study. *J. Neuroeng. Rehabil.*, **5**, 29.
8. Lu, J.P., Wang, Y., Sliter, D.A., Pearce, M.M.P. and Wojcikiewicz, R.J.H. (2011) RNF170 protein, an endoplasmic reticulum membrane ubiquitin ligase, mediates inositol 1,4,5-trisphosphate receptor ubiquitination and degradation. *J. Biol. Chem.*, **286**, 24426–24433.
9. Mikoshiba, K. (2007) IP3 receptor/Ca2+ channel: From discovery to new signaling concepts. *J. Neurochem.*, **102**, 1426–1446.
10. Nakamura, N. (2011) The role of the transmembrane RING finger proteins in cellular and organelle function. *Membranes*, **1**, 354–393.
11. Valdmanis, P.N., Dupré, N., Lachance, M., Stochmanski, S.J., Belzil, V.V., Dion, P.A., Thiffault, I., Brais, B., Weston, L., Saint-Amant, L. *et al.* (2011) A mutation in the RNF170 gene causes autosomal dominant sensory ataxia. *Brain*, **134**, 602–607.
12. Valdmanis, P.N., Brunet, D., St-Onge, J., Weston, L., Rouleau, G.A. and Dupré, N. (2006) A founder haplotype for autosomal dominant sensory ataxia in Eastern Canada. *Neurology*, **67**, 2239–2242.
13. Valdmanis, P.N., Simões Lopes, A.A., Gros-Louis, F., Stewart, J. D., Rouleau, G.A. and Dupré, N. (2004) A novel neurodegenerative disease characterised by posterior column ataxia and pyramidal tract involvement maps to chromosome 8p12–8q12.1. *J. Med. Genet.*, **41**, 634–639.
14. Wright, F.A., Lu, J.P., Sliter, D.A., Dupré, N., Rouleau, G.A. and Wojcikiewicz, R.J.H. (2015) A point mutation in the ubiquitin ligase RNF170 that causes autosomal dominant sensory ataxia destabilizes the protein and impairs inositol 1,4,5-trisphosphate receptor-mediated Ca^{2+} signaling. *J. Biol. Chem.*, **290**, 13948–13957.
15. Curry, D.L., Bennett, L.L. and Grodsky, G.M. (1968) Dynamics of insulin secretion by the perfused rat pancreas. *Endocrinology*, **83**, 572–584.
16. Wollheim, C.B. and Sharp, G.W. (1981) Regulation of insulin release by calcium. *Physiol. Rev.*, **61**, 914–973.
17. Hamers, F.P.T., Koopmans, G.C. and Joosten, E.A.J. (2006) CatWalk-assisted gait analysis in the assessment of spinal cord injury. *J. Neurotrauma*, **23**, 537–548.
18. Whishaw, I., Haun, F. and Kolb, B. (1999) Analysis of behavior in laboratory rodents. In Windhorst, U. and Johansson, H. (eds), *Modern Techniques in Neuroscience Research*. Springer, Berlin, Heidelberg, pp. 1243–1275.
19. Neumann, M., Wang, Y., Kim, S., Hong, S.M., Jeng, L., Bilgen, M. and Liu, J. (2009) Assessing gait impairment following experimental traumatic brain injury in mice. *J. Neurosci. Methods*, **176**, 34–44.
20. Cendelin, J., Voller, J. and Vozeh, F. (2010) Ataxic gait analysis in a mouse model of the olivocerebellar degeneration. *Behav Brain Res*, **210**, 8–15.
21. Cheret, C., Willem, M., Fricker, F.R., Wende, H., Wulf-Goldenberg, A., Tahirovic, S., Nave, K.-A., Saftig, P., Haass, C., Garratt, A.N. *et al.* (2013) Bace1 and Neuregulin-1 cooperate to control formation and maintenance of muscle spindles. *EMBO J.*, **32**, 2015–2028.
22. Simon, D., Seznec, H., Gansmuller, A., Carelle, N., Weber, P., Metzger, D., Rustin, P., Koenig, M. and Puccio, H. (2004) Friedreich ataxia mouse models with progressive cerebellar and sensory ataxia reveal autophagic neurodegeneration in dorsal root ganglia. *J. Neurosci.*, **24**, 1987–1995.
23. Chen, X.J., Levedakou, E.N., Millen, K.J., Wollmann, R.L., Soliven, B. and Popko, B. (2007) Proprioceptive sensory neuropathy in mice with a mutation in the cytoplasmic Dynein heavy chain 1 gene. *J. Neurosci.*, **27**, 14515–14524.
24. Kai, S. and Nakabayashi, K. (2013) Evoked EMG makes measurement of muscle tone possible by analysis of the H/M ratio. In Turker, H. (ed.), *Electrodiagnosis in New Frontiers of Clinical Research*. InTech, Rijeka, Croatia, pp. 195–212.
25. Khasnis, A. and Gokula, R.M. (2003) Romberg's test. *J Postgrad. Med.*, **49**, 169–172.
26. Kasumu, A.W., Liang, X., Egorova, P., Vorontsova, D. and Bezprozvanny, I. (2012) Chronic suppression of inositol 1,4,5-triphosphate receptor-mediated calcium signaling in cerebellar purkinje cells alleviates pathological phenotype in spinocerebellar ataxia 2 mice. *J. Neurosci.*, **32**, 12786–12796.
27. Zhuchenko, O., Bailey, J., Bonnen, P., Ashizawa, T., Stockton, D.W., Amos, C., Dobyns, W.B., Subramony, S.H., Zoghbi, H.Y. and Lee, C.C. (1997) Autosomal dominant cerebellar ataxia (SCA6) associated with small polyglutamine expansions in the alpha 1A-voltage-dependent calcium channel. *Nat. Genet.*, **15**, 62–69.
28. Yue, Q., Jen, J.C., Nelson, S.F. and Baloh, R.W. (1997) Progressive ataxia due to a missense mutation in a calcium-channel gene. *Am. J. Hum. Genet.*, **61**, 1078–1087.
29. Metzger, M.B., Hristova, V.A. and Weissman, A.M. (2012) HECT and RING finger families of E3 ubiquitin ligases at a glance. *J. Cell Sci.*, **125**, 531–537.
30. Chen, G., Patten, C., Kothari, D.H. and Zajac, F.E. (2005) Gait differences between individuals with post-stroke hemiparesis and non-disabled controls at matched speeds. *Gait Posture*, **22**, 51–56.
31. Cirstea, M.C. and Levin, M.F. (2000) Compensatory strategies for reaching in stroke. *Brain*, **123**(Pt 5), 940–953.
32. Bruijn, S.M., Meijer, O.G., Beek, P.J. and van Dieen, J.H. (2010) The effects of arm swing on human gait stability. *J. Exp. Biol.*, **213**, 3945–3952.
33. Collins, S.H., Adamczyk, P.G. and Kuo, A.D. (2009) Dynamic arm swinging in human walking. *Proc. Biol. Sci.*, **276**, 3679–3688.
34. Meyns, P., Bruijn, S.M. and Duysens, J. (2013) The how and why of arm swing during human walking. *Gait Posture*, **38**, 555–562.
35. Grillner, S., Ekeberg, El Manira, A., Lansner, A., Parker, D., Tegner, J. and Wallen, P. (1998) Intrinsic function of a neuronal network - a vertebrate central pattern generator. *Brain Res. Brain Res. Rev.*, **26**, 184–197.
36. Duysens, J. and Van de Crommert, H.W. (1998) Neural control of locomotion; the central pattern generator from cats to humans. *Gait Posture*, **7**, 131–141.
37. Talpalar, A.E., Bouvier, J., Borgius, L., Fortin, G., Pierani, A. and Kiehn, O. (2013) Dual-mode operation of neuronal networks involved in left-right alternation. *Nature*, **500**, 85–88.
38. Iwasato, T., Katoh, H., Nishimaru, H., Ishikawa, Y., Inoue, H., Saito, Y.M., Ando, R., Iwama, M., Takahashi, R., Negishi, M. *et al.* (2007) Rac-GAP alpha-chimerin regulates motor-circuit formation as a key mediator of EphrinB3/EphA4 forward signaling. *Cell*, **130**, 742–753.
39. Moeller, J.J., Macaulay, R.J., Valdmanis, P.N., Weston, L.E., Rouleau, G.A. and Dupre, N. (2008) Autosomal dominant sensory ataxia: a neuroaxonal dystrophy. *Acta Neuropathol.*, **116**, 331–336.